Formation of C-A-S-H phases from the interaction between concrete or cement and bentonite

RAÚL FERNÁNDEZ*, ANA ISABEL RUIZ AND JAIME CUEVAS

Department of Geology and Geochemistry, Faculty of Sciences, Autonomous University of Madrid, Spain

ABSTRACT: Concrete and bentonite are being considered as engineered barriers for the deep geological disposal of high-level radioactive waste in argillaceous rocks. Three hydrothermal laboratory experiments of different scalable complexity were performed to improve our knowledge of the formation of calcium aluminate silicate hydrates (C-A-S-H) at the interface between the two materials: concrete-bentonite transport columns, lime mortar-bentonite transport columns and a portlandite- (bentonite and montmorillonite) batch experiment. Precipitation of C-A-S-H was observed in all experiments. Acicular and fibrous morphologies with certain laminar characteristics were observed which had smaller Ca/Si and larger Al/Si ratios with increasing temperature and lack of accessory minerals. The compositional fields of these C-A-S-H phases formed in the experiments are consistent with Al/(Si+Al) ratios of 0.2–0.3 described in the literature. The most representative calcium silicate hydrate (C-S-H) phase from the montmorillonite–cement interface is Al-tobermorite. Structural analyses revealed a potential intercalation or association of montmorillonite and C-A-S-H phases at the pore scale.

The concrete–bentonite interactions, and more general, concrete–clay interactions, have been studied as part of the expected geochemical reactions occurring within the composite engineered barriers in high-level radioactive waste in deep geological repositories (*e.g.* US DOE, 2014). The long-term result of such interactions has to be evaluated in order to tackle the impact on the mineralogical and physical-chemical properties at the interface of both materials that could compromise their safety functions in the long-term (Gaucher & Blanc, 2006; Savage *et al.*, 2007).

Experimental evidence demonstrates that the alkaline plume will generate partial dissolution of montmorillonite, formation of illite-smectite mixed layers and precipitation of Na/K-zeolites and trioctahedral Mg smectite (Sánchez *et al.*, 2006; Fernández *et al.*,

2014b) under hyperalkaline conditions (pH>12.5). The formation of calcium silicate hydrates (C-S-H), Mg hydroxides and Mg clays (Diamond *et al.*, 1963; Rao & Rajasekaran, 1996; Fernández *et al.*, 2006; Dauzères *et al.*, 2010), however, predominates under moderate alkaline conditions (pH<12.5) or in the presence of lime. The nature of the reaction products depends largely on the experimental conditions: *e.g.* temperature, pH, composition of clays and solution and duration of the reaction (Dauzères *et al.*, 2010; Fernández *et al.*, 2010). In addition to that, concrete materials located in natural clay environments are subjected to carbonation and sulfate precipitation near the clay–concrete interface (Jenni *et al.*, 2014) or at the concrete interface under carbonic environment, where calcite precipitation replacing initial C-S-H minerals and portlandite have been described (Dauzères *et al.*, 2014).

Accessory minerals in bentonite affect the reactivity and participate in the precipitation of C-S-H phases, by

*E-mail: raul.fernandez@uam.es

means of several reactions on silicate mineral surfaces. These C-S-H phases exhibit different morphologies (typically fibrous or laminar) and chemical compositions. They have been observed within a large range of Ca/Si ratios that may extend from 0.8 or even lower, to near 2 (Cuevas *et al.*, 2006).

At laboratory scale, the C-S-H phases obtained in clay–concrete environments are difficult to identify because they usually precipitate accompanied by other secondary minerals at the µm–nm pore scale. C-S-H phases are amorphous or poorly crystalline and are not well preserved at ambient conditions because they become carbonated. Often, the C-S-H phases are identified as tobermorite-like when they exhibit low Ca/Si ratios (0.66–0.83) and as "jennite-like" phases at high Ca/Si ratios (1.25–1.50) (Nonat, 2004). In fact, thermodynamic solid-solution models tend to include this structural approach (Kulik, 2011).

An additional fact that complicates the identification of C-S-H phases is the partial substitution of Si by Al to form calcium aluminium silicate hydrates (C-A-S-H) added to the replacement of Ca by Na and Mg in these phases (Komarneni *et al.*, 1987; Jackson *et al.*, 2013). These Al-substituted tobermorites have been studied mostly during the hydration of ordinary Portland Cement (OPC) pastes in the presence of sodium aluminate (Sun *et al.*, 2006; Russias *et al.*, 2008) and not in the context of clay environments. This is because it would be difficult to identify their 11–13 Å XRD basal spacing, which is very similar to smectitic 2:1 sheet silicate minerals characteristic of bentonites and other low-permeability clay rocks. In terms of chemical composition, they could be distinguished from Al-rich clay minerals by the limited Al/(Si+Al) ratio, which ranges between 0.2 and 0.3 (Pardal *et al.*, 2009).

Magnesium silicate hydrate phases (M-S-H) may form also when large Mg contents are available in the reaction water. The M-S-H phases exhibit Mg/Si ratios of between 4:1 and 1:2 and have structures which are different from C-S-H phases. M-S-H with Mg/Si ratios of $\sim$0.6 appear to be structurally comparable to nanocrystalline turbostratic 2:1 Mg-Si phyllosilicates (Roosz *et al.*, 2015). Although both types of phases may coexist, C-S-H contains little Mg while M-S-H contains little Ca (Brew & Glasser, 2005).

The importance of the C-S-H or C-A-S-H identification in the clay–concrete reaction environment relies on the reaction products that will allow long-term prediction of the reactivity of the system. Although efforts have been made recently to establish consistent thermodynamic properties of phases in the system $CaO–SiO_2–H_2O$ (Blanc *et al.,* 2010), geochemical models usually consider a wide range of possible C-S-H and C-A-S-H phases with varying compositions based on standard databases or solid solution models, but do not include sound thermodynamic data to model C-A-S-H (Grandia *et al.*, 2010; Savage *et al.*, 2011). In other cases, analogues of C-A-S-H, such as prehnite (Soler & Mäder, 2010; Soler, 2013) or katoite (Marty *et al.*, 2009) have been used successfully in prediction models when such phases are expected to form.

Therefore, the objective of the present study was to characterize the typical C-S-H or C-A-S-H phases observed in the bentonite–cementitious interface materials sampled from various existing experiments with different scale size, time and experimental conditions in order to determine which compositions and structures dominate in such environments. This was done to produce first-stage research looking for a consistent C-A-S-H composition to further explore its thermodynamic properties for prediction applications.

MATERIALS AND METHODS

In the present study, results from three types of laboratory experiments were considered. The three experiments exhibited different complexity conditions and the exhaustive description of the experimental procedures has been published elsewhere (Cuevas *et al.*, 2016; Fernández *et al.*, 2014a; Torres *et al.*, 2009). A brief description of the three experimental setups is given here.

The internal coherence between the three experiments was maintained by use of a common material, FEBEX bentonite which, extracted from the Cortijo de Archidona (Almería), is the Spanish reference material for radioactive waste disposal (Villar *et al.*, 2006). It is a well known bentonite, studied and characterized extensively (Fernández *et al.*, 2004; Caballero *et al.*, 2005). The FEBEX bentonite contains $\sim$92% of montmorillonite implying a large cation exchange capacity (CEC) (of $\sim$100 meq/100 g) and large specific surface area ($\sim$61 m^2/g external surface area and 725 m^2/g total surface area). The bentonite contains accessory quartz, cristobalite, feldspars and plagioclase, and traces of carbonates and soluble salts such as gypsum and halite.

EXPERIMENTAL

Medium cells

The medium cells comprise a series of laboratory column experiments performed under the NF-PRO and

TABLE 1. Chemical analysis of the CEM I 42.5 R/SR cement.

Chemical composition (%)	SiO_2	Al_2O_3	Fe_2O_3	CaO (total)	MgO	SO_3	Na_2O	K_2O	CaO (free)
CEM-I-SR	19.6	4.43	4.27	65.6	0.95	3.29	0.11	0.28	1.92

PEBS EU Projects (Turrero *et al.*, 2011). The objective of these experiments was to investigate the reactivity at the concrete–bentonite interface. Each column contained compacted FEBEX bentonite and a high-pH concrete, and the reaction time varied from 6 months to 6.5 y. The results extracted in the present study were taken from cells HB4 and HB5, performed for 4.5 and 6.5 y, respectively. Both cells included a cylindrical concrete block 70 mm in diameter and 30 mm tall in direct contact with a compacted FEBEX bentonite column 70 mm in diameter and 71.5 mm tall.

Concrete and bentonite were inserted into a Teflon sleeve and sealed with stainless steel rings to prevent deformation. The cells were heated at 100°C from the bottom (bentonite side) and hydrated from the top (concrete side), simultaneously. These conditions simulate the heat emitted by the radioactive waste from the canister side and the hydration to the engineered barriers system from the host-clay formation side.

Hydration was introduced by means of a synthetic infiltration saline solution, representative of a Spanish clayey formation, which was circulated from a pressurized reservoir initially set at 5 bar with nitrogen. The reservoir was maintained at room temperature (25°C). The infiltration solution had the following composition: 7.0×10^{-2} M SO_4^{2-}, 2.3×10^{-2} M Cl^-, 1.3×10^{-1} M Na^+, 8.2×10^{-3} M Mg^{2+}, 1.1×10^{-5} M $Fe^{(3+/2+)}$, 8.2×10^{-4} M K^+, 1.1×10^{-2} M Ca^{2+}, 2.7×10^{-4} M $SiO_{2(aq)}$ and 1.8×10^{-3} M HCO_3^- at pH 7.5.

The concrete composition was based on a sulfo-resistant OPC CEM I 42.5 R/SR type of cement without mineral additions. The cement composition was based on that used in the repository of El Cabril (Cordoba, Spain) for low- and medium-level radioactive wastes (Andrade *et al.*, 2006). The chemical composition of the cement paste is shown in Table 1. The dry density of the concrete was, on average, 2.22 ± 0.01 g/cm³. Its water content was $2.6 \pm 0.8\%$ before, and $6.4 \pm 0.6\%$ after saturation.

In order to produce the cylindrical bentonite block, a sample consisting of 504.9 g of FEBEX bentonite, already dried at 60°C and sieved to 5 mm, was compacted uniaxially by applying a pressure of 43 MPa. Deionized water was added to produce a saturated sample and the dry density value obtained was 1.65 g/cm³.

Dismantling of cells HB4 and HB5 involved a complex sectioning of both columns to study the hydrogeochemical processes across the columns. The present study focused only on samples taken from the concrete–bentonite interface (*i.e.* <3 mm from the interface). Detailed descriptions of these experiments and the results obtained for cells HB1–HB4 have been published by Torres *et al.* (2009) and Cuevas *et al.* (2012).

Small cells

The small cells are also cylindrical-column experiments performed in series. These experiments were performed under the auspices of the PEBS EU Project. Six different columns were prepared using either natural FEBEX bentonite or a pre-treated FEBEX bentonite free of exchangeable Mg. The pre-treated sample was prepared in order to work with a bentonite that resumes its geochemical prevailing state after 1000–3000 y under repository conditions, considering the calculations performed by Samper *et al.* (2010). The advantage of using lime mortar instead of concrete is that the complexity of the chemical composition is reduced and the formation of C-A-S-H phases can be better tied to the original source of alkalinity.

Only three interface samples of the six experiments are shown in the present study: cell 3, which contains the lime mortar in the upper part, pre-treated bentonite in the middle and magnetite at the bottom of the column; cell 4, with the same components but substituting the pre-treated sample for natural bentonite; and cell 5, which includes pre-treated bentonite and excludes magnetite.

The experiments were performed in cylindrical Teflon cells with an internal diameter of 50 mm and an inner length of 25 mm. The upper closing was made of stainless steel and was connected to a pressurized water reservoir from which a saline solution, of identical composition to that used for the medium

cells, was infiltrated into the column. The reservoir was initially pressurized at 5 bar with nitrogen.

The lime mortar was formulated as a 2:1 quartz-sand/CaO mixture. Quartz-sand was sieved to <0.5 mm and CaO was obtained by calcination at 950°C of a commercial $Ca(OH)_2$ reagent Panreac™ P.A. grade. CaO was allowed to quench inside a glove-box with a N_2 atmosphere and using NaOH pellets as a trap for CO_2.

The lime mortar produced had pH of 12.6, a water content of 22.9 wt.% and a dry density of 1.55 g/cm³. The sample was cylindrical with a diameter of 50 mm and a height of 6 mm.

The cylindrical bentonite blocks were again compacted to reach a dry density of 1.65 g/cm³. They were placed in direct contact with the lime mortar and the height of the column was covered up to 25 mm, except when magnetite powder was inserted which reduced the height by 2 mm.

All the experiments were run at a constant reaction temperature of 60°C, which is the temperature expected at the concrete–bentonite interface in the simulated repository case 1000–3000 y after disposal. The reaction time for all experiments was ~18 months. The experiments were discussed by Cuevas *et al.* (2013, 2014a,b) and by Torres *et al.* (2014). A detailed description of the experimental setup and major findings has appeared in the paper by Cuevas *et al.* (2016).

Batch experiments

These experiments assume a more simplified stage of alkaline source than the experiments described previously. Powder FEBEX bentonite and portlandite were mixed in water protected from atmospheric CO_2 in closed batch reactors and left to react for ~2 months.

Two types of samples were used: the natural FEBEX bentonite ground to a grain size of <1 mm and its extracted size fraction <2 μm, which consisted mostly of montmorillonite. The mixes were prepared at two montmorillonite/portlandite molar ratios (2:1 and 3:1), and two reaction temperatures were applied: 60 and 120°C. Therefore, a total of eight experiments were performed.

Once the programmed reaction time had been attained, the reactors were opened and the solid and liquid phases were separated by centrifugation. The solid phase was dried in a desiccator to prevent carbonation, and ground again to powder for physico-chemical analysis. The description of these latter

TABLE 2. Summary of description of experiment types and conditions.

Experiment type	Number of experiments	Materials	Dimensions	Hydration	T (°C)	Time
Medium cells	2	Concrete CEM-I-SR	Cylindrical 70 × 30 mm	Clayey saline solution Na^+-SO_4^{2-} dominant	Gradient 100°C at bottom (bentonite) ~40°C at the interface	4.5 and 6.5 y
		FEBEX bentonite 1.65 g/cm³ dry density	70 × 71.5 mm			
Small cells	3	Lime mortar 2:1 quartz-sand/CaO mixture	50 × 6 mm		Constant 60°C	18 months
		Natural FEBEX bentonite Pre-treated FEBEX (Mg-depleted) 1.65 g/cm³ dry density	50 × 25 mm			
Batch experiments	8	FEBEX bentonite FEBEX bentonite <2 μm (montmorillonite)	Powder	Portlandite solution $Ca(OH)_2$ at molar ratios of 2:1 and 3:1 for mont/portl.	60 and 120°C	2 months

experiments and the results obtained can be found in Fernández *et al.* (2014a). A summary of conditions applied in each experiment is shown in Table 2.

Analytical techniques

All procedures for sample preparation were performed in a sealed glove-box at $N_{2(g)}$ atmosphere. In addition, the absence of $CO_{2(g)}$ was achieved by means of NaOH pellet traps in the glove-box. Drying of samples was performed in vacuum and isolated from laboratory air. Rehydration of clay and cement materials in order to pre-condition the samples for XRD experiments was performed by equilibrating the samples for 48 h in a 50% relative humidity chamber (controlled by $MgNO_3$-saturated solution at 25°C).

Scanning Electron Microscopy (SEM) was performed using a Philips XL 30 instrument coupled to an Energy Dispersive X-ray analyser (EDX). The accuracy of the EDX analyses cannot be evaluated for these samples due to their heterogeneity. Most of the analyses were done on small C-A-S-H mineral surfaces surrounded by clay substrates or matrices of different composition that could have interfered with the analytical determinations. Consequently, all EDX analyses should be read with caution and with a safe margin allowed for error. In any case, the compositional trends as a function of the conditions applied in each experiment are marked.

X-ray diffraction (XRD) was performed using a Philips X'pert PRO diffractometer with an X-celerator detector over the range 3°70°2θ using Cu-$K\alpha_1$ radiation ($\lambda = 1.54056$ Å) and a Ge monochromator with divergence and reception slits of 2 and 0.6 mm, respectively. The diffractometer operated at 40 kV and 40 mA.

Solid-state Cross-Polarization Magic Angle Spinning ^{29}Si Nuclear Magnetic Resonance (CP/MAS-NMR) spectra were acquired using a Bruker AV-400-WB spectrometer equipped with a 4 mm MAS-NMR probe, with the samples spinning at a rate of ~10 kHz. The operating frequency was 79.49 MHz, using 60 s excitation pulses (π/2) at 50 kHz. The chemical shifts of ^{29}Si resonances were evaluated in relation to kaolin (–91.5 ppm) and tetramethylsilane (TMS) as secondary and primary references, respectively.

RESULTS AND DISCUSSION

Scanning Electron Microscopy (SEM-EDX)

Morphological and chemical analyses performed by SEM-EDX on selected samples at the interface of experiments HB4 and HB5 in the medium cells revealed mostly acicular and needle-like C-A-S-H morphologies, contained in Si-rich crusts (formed by dissolution of clay minerals in pores), and exhibiting a wide range of Ca/Si atomic ratios in their chemical compositions. Accurate analysis of these phases in the concrete–bentonite interface by EDX is particularly difficult due to the complex matrix that surrounds the C-A-S-H phases or acts as supports for their nucleation. The C-A-S-H phases grow on Si-rich substrates and are accompanied by other secondary minerals such as carbonates (on the bentonite side) and ettringite (on the concrete side).

Curved and helicoidally twisted 10–20 μm long fibres were detected in the HB4 experiment, precipitating on the Si-rich crust formed on the bentonite side of the interface (Fig. 1A–D). The Si-rich crust surrounds undistinguished fibres growing on pores (Fig. 1A). Details of the morphology of these fibres is presented at higher magnification (Fig. 1B, C, D). In HB5, thin fibres are seen clearly to have grown from the crust formed, some of them containing nodules at the middle and at the margins of the fibre (Fig. 1E, F). Experiments on small cells produced fewer pores at the interface; subsequently, with a few exceptions (*e.g.* Fig. 1G), the typical C-A-S-H morphologies were not observed (Fig. 1H).

The formation of C-A-S-H in the batch experiments was extensive, and the morphology of these phases varied according to the experimental conditions. At 60°C, only in the experiment with bentonite and montmorillonite/portlandite molar ratio of 2:1, the C-A-S-H phases were associated with clay aggregates. These phases show short needle-like crystals ~10 μm long (Fig. 1I) with Ca/Si and Al/Si atom ratios of 1.27 ± 0.24 and 0.24 ± 0.05, respectively (analyses based on ten EDX point analyses on the surface of these crystals). Small spherical nodules also precipitated as a result of the bentonite-portlandite reaction. These nodules were well mixed with the clay aggregates; therefore the clay composition might have affected the EDX analyses. The nodules belong to calcium aluminates phases, also detected by XRD.

Rounded clusters of bladed crystals were observed at 120°C in experiments using bentonite with a montmorillonite/portlandite ratio of 2:1 (Fig. 1J). By increasing the montmorillonite/portlandite ratio to 3:1, C-A-S-H phases occurred with a more fibrous aspect, mixed with clay aggregates (Fig. 1K). At 120°C, using montmorillonite and montmorillonite/portlandite mixtures with ratios of 2:1 and 3:1, rounded clusters of bladed crystals and fibrous morphologies were observed (Fig. 1L).
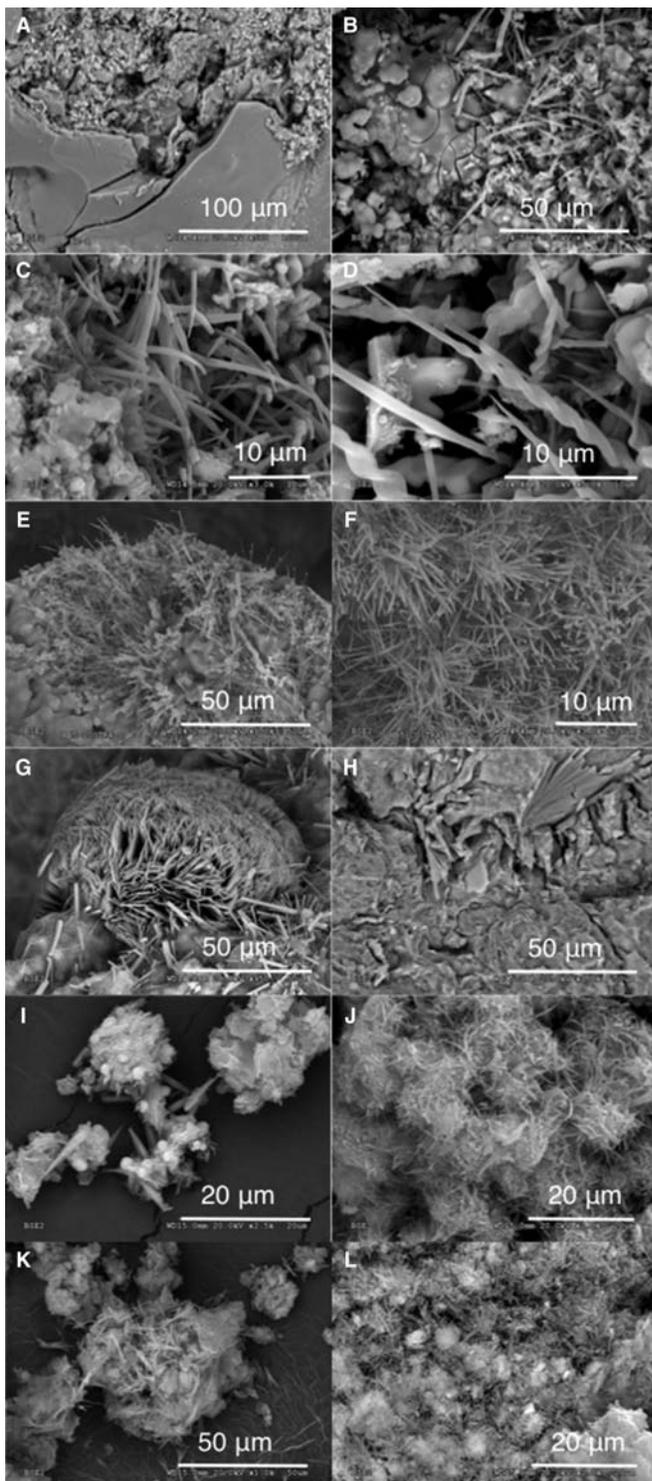
FIG. 1. SEM images of the reacted samples: (A, B, C, D) HB4 cell; (E, F) HB5 cell; (G) small cell 3; (H) small cell 5; (I) bentonite 60°C, montmorillonite/portlandite 2:1; (J) bentonite 120°C, montmorillonite/portlandite 2:1; (K) bentonite 120°C, montmorillonite/portlandite 3:1; and (L) montmorillonite 120°C, montmorillonite/portlandite 2:1.
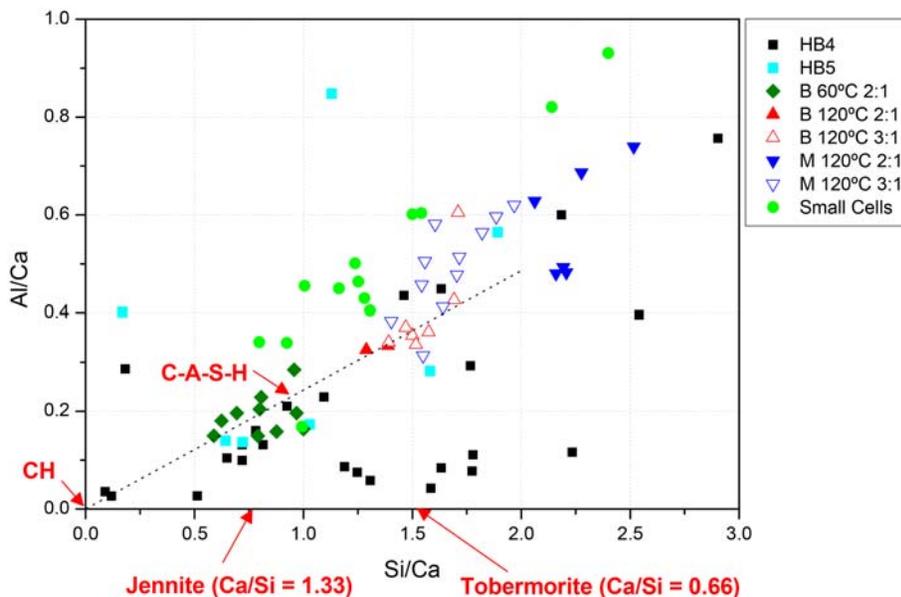
FIG. 2. Plots of the Al/Ca *vs.* Si/Ca atomic ratios for the EDX analyses of C-A-S-H in selected samples of the three experiments. The Ca/Si ratios shown for tobermorite and jennite are in agreement with values from Nonat (2004). CH = portlandite. HB4 and HB5 correspond to medium cell experiments; B = bentonite, M = montmorillonite, 2:1 and 3:1 are the montmorillonite/portlandite molar ratios in batch experiments.

An attempt to determine the chemical composition of C-A-S-H phases was made for all the samples obtained in the three experiments by EDX analysis. The results were projected in scatter diagrams using Al/Ca *vs.* Si/Ca atom ratios (Fig. 2). The considerable dispersion of the data points is attributed to the fact that the EDX analysis is semi-quantitative and also to the substrate or surrounding minerals phases which can interfere with and contribute to the chemical composition. As a result, contributions mainly of Si and Al from the clay matrix, acting as substrate or support for C-A-S-H phases, is assumed for those data points at the right and top end sides of the diagram. On the other hand, the chemical composition of those data points close to the origin, which typically represent compositions of early-stage hydration of C-S-H gels that form from portlandite (CH), could be contaminated by excess Ca from the surrounding carbonates.

The general trend indicates that Al and Si increase in the C-A-S-H composition when the temperature increases. The medium-cell experiments (temperature at the concrete–bentonite interface was ~40°C) present scattered data. Experiments performed at 60°C (either in the small cells or in the batch reactor with bentonite at a montmorillonite/portlandite ratio of 2:1) show consistent C-S-H compositions within the Ca/Si ratio

range of jennite–tobermorite. At 120°C, the Al/Ca and Si/Ca ratios in the C-A-S-H compositions obtained in the batch experiments increased. This effect could be related to the decrease of portlandite solubility with increasing temperature and hence its lower availability to react. Furthermore, the Al/Ca and Si/Ca ratios also increased when montmorillonite was used instead of bentonite. The increase in Al and Si could be attributed to the enhancement of montmorillonite reactivity with temperature.

Powder XRD

One of the aims of the present study was to determine the presence of C-A-S-H phases in different experiments containing cement materials and bentonite interfaces. X-ray diffraction patterns of selected samples of each of the three experiments analysed compared to the original FEBEX montmorillonite are shown in Fig. 3.

The samples from the HB5 (6.5-y experiment) cement–bentonite interface have more complex mineralogy than other experiments. The main differences are due to the presence of carbonates phases, calcite and minor aragonite (not marked). Nevertheless, most of the asymmetric *hk*0 reflections (4.49, 3.00, 2.57 and

1.70 and 1.50 (060) Å), characteristic of the turbostratically disordered layer structures of montmorillonite (Ufer *et al.*, 2004) are still present in the same angular positions. This means that the structure of the montmorillonite remained similar to the original FEBEX bentonite.

At ~30°2θ, the *d* spacings of broad reflections centred at between 3.04 and 3.08 Å reveal the possible presence of disordered C-S-H tobermorite-type phases (clino-tobermorite; Henmi & Kusachi, 1992) in the mortar interfaces at small cells and in the portlandite-montmorillonite batch experiments. Only in the 120°C batch experiments was a series of reflections corresponding to ordered orthorhombic tobermorite (11.5, 5.4, 3.08, 2.97, 2.86 Å) identified (Merlino *et al.*, 1999). Apart from the detection of these phases and the apparent preservation of montmorillonite structures, the diffraction maximum that corresponds to the 001 basal spacing of the montmorillonite was observed at 12–13 Å. This *d* spacing value is very small considering that calcium should be in the montmorillonite interlayer (typically identified at 15 Å) in contact with hydrated cement phases. These reflections are very broad and can overlap with the angles that might also indicate C-S-H or C-A-S-H of tobermorite type (14–11–9 Å type; Sun *et al.*, 2006). In the 120°C experiments, a sharp

diffraction maximum at 11.5 Å was observed which departs from the pure C-S-H 11.0 Å, and has been related to the presence of Al-tobermorite with a ~0.2 Al/(Si+Al) ratio (Jackson *et al.*, 2013).

In order to discriminate the XRD reflections that belong to montmorillonite from those belonging to the C-A-S-H phases, powder samples from the batch experiments were mixed with liquid ethylene-glycol (EG) at a ratio of 1:1 wt.%. The XRD patterns of EG-treated samples of the original montmorillonite (EG-Mmt) and samples after reaction at 60 and 120°C were compared to the non EG-treated samples (Fig. 4). Disordered C-S-H-Mmt components in both samples at 60 and 120°C showed an incomplete but apparent regular swelling (the 005 reflection is consistent with the 001 basal spacing). The low-angle reflection is thus consistent with an intercalation or association at the nanoscale of tobermorite and montmorillonite (expandable), although this hypothesis should be studied further. Besides, Al-tobermorite C-A-S-H (ordered), behaves as a discrete phase with XRD-invariant reflections.

Nuclear magnetic resonance

Analytical data of the chemical shifts of ^{29}Si MAS NMR spectra in selected samples of the three
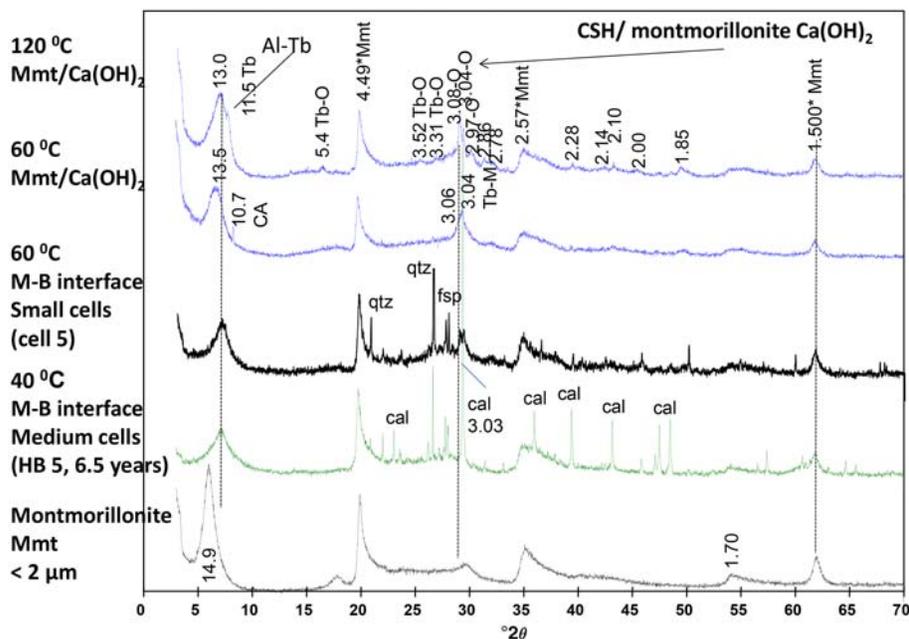

FIG. 3. Powder XRD patterns of samples from selected experiments. Al-Tb: Al-tobermorite, Tb-O: ordered tobermorite; Tb-M: disordered monoclinic tobermorite; qtz: quartz, fsp: feldspars; cal: calcite. Numbers indicate *d* spacings (Å).
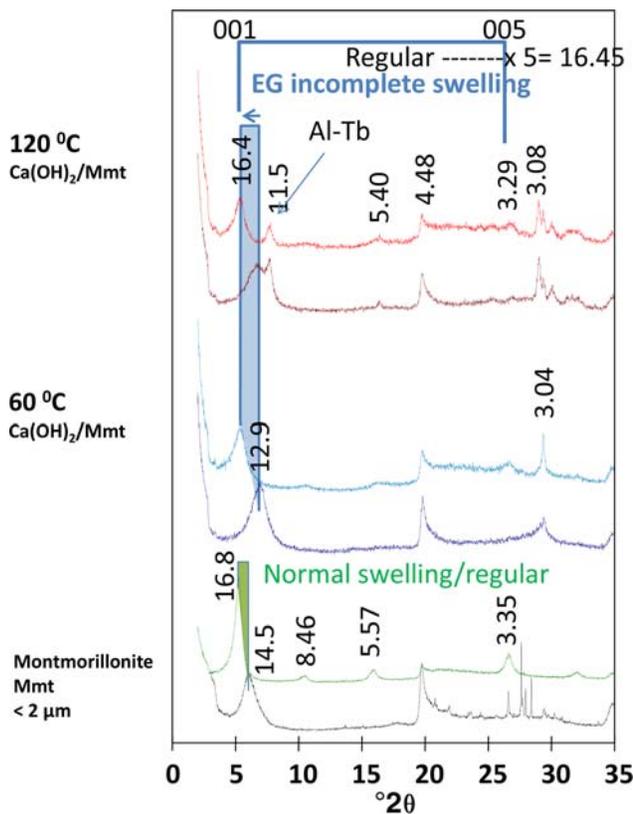
F<small>IG</small>. 4. Ethylene-glycol treated powder XRD patterns compared to the original (non-treated) powder patterns in lime-montmorillonite batch experiments. Mmt: montmorillonite, Al-Tb: Al-tobermorite. Numbers indicate *d* spacings (Å).

experiments and in the unreacted FEBEX montmorillonite (Mmt) are shown in Fig. 5A–C and in Table 3.

In the original FEBEX bentonite, the main signal at $\delta \approx -93$ ppm is attributed to ^{IV}Si in montmorillonite (Thompson, 1984). This ^{IV}Si signal is attributed to Q^3 Si (Lippmaa *et al.*, 1980). The corresponding signal has a rather broad line indicating local disordering of the Si environment within the montmorillonite structure. Moreover, the presence of a small shoulder in the main signal at $\delta \approx -88$ ppm indicates partial substitution of ^{IV}Si by ^{IV}Al in the tetrahedral sheets (Sánchez *et al.*, 2006). As a result, the chemical shift of the signals from Si nuclei located near these ^{IV}Al atoms (Q^3 [1Al] signal) is moved slightly down field.

In small-cell and batch experiments, two new signals were observed other than the montmorillonite resonances (~-93 ppm), compared to the original FEBEX montmorillonite spectrum. The new signals appeared in the –81 to –85 ppm region and are assigned to C-S-H phases (Pomakhina *et al.*, 2012),

as already observed by XRD. The chemical shift of ^{29}Si at ~-85 ppm was assigned to tetrahedral Si, which is bonded in the middle of silicate chains (Q^2). When aluminium was incorporated into the silicate chain as a bridging tetrahedron, an additional peak was observed at ~-82 ppm (Q^2 [1Al]; Richardson *et al.*, 1993).

The NMR spectrum of the D1-C sample (located at the cement–bentonite interface), also contained a chemical shift at –107.4 ppm, which corresponds to quartz (de Jong *et al.*, 1987).

The best described structure of C-S-H is similar to tobermorite. However, the tobermorite-like structure of C-S-H does not describe all systems equally well. The C-S-H may consist of two or three different phases; the tobermorite and related tobermorite-jennite models were developed mainly in systems at equilibrium, achieved at very long reaction times (several weeks or months) and/or elevated temperatures (Richardson *et al.*, 1993; Cong & Kirkpatrick, 1996).
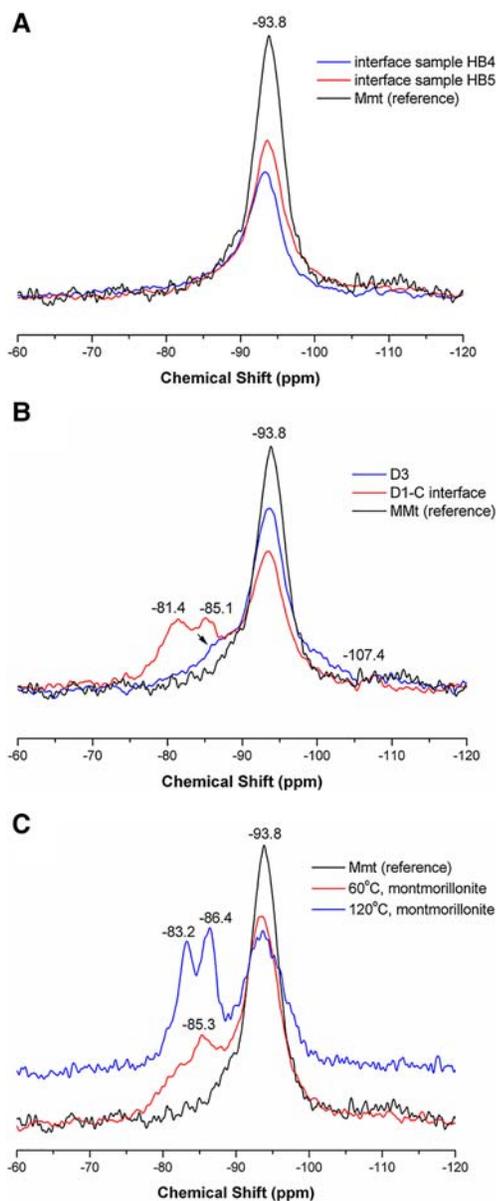
structures with a high Ca/Si ratio (1.5–1.2; Brunet *et al.*, 2004). Therefore, in this case, the C-S-H structures are characterised by long chains and tobermorite-like structure with a low Ca/Si ratio (0.88–0.66).

In addition, the ^{29}Si NMR analysis (Fig. 5) indicates the presence of alumina tetrahedra in the silicate chain (Q^2 [1Al] signals). Hence, the NMR results indicate the presence of C-S-H phases with a limited substitution of Al^{3+} for Si^{4+}, and therefore these phases are characterized as C-A-S-H.

SUMMARY AND CONCLUSIONS

The C-S-H-type phases formed in experiments from cement–bentonite interaction have complex chemical composition, mainly due to the intimate mixture with existing clay minerals. When the experimental conditions reproduce more realistic scenarios of interactions between the concrete and bentonite barriers of a radioactive waste repository, the characterization of crystalline disordered C-S-H phases formed at low temperature (<60°C) becomes more difficult. Their characterization is also masked by the formation of calcium carbonates in the mixture. Fibrous or acicular morphologies are distinguished when porous space is available, but according to the present work they do not have fixed compositions. However, the most frequent values of the Ca/Si ratios in C-A-S-H crystals obtained from SEM-EDX analyses are 0.5–0.8 (tobermorite-like). Furthermore, XRD data reveal the predominance of tobermorite-like phases. The NMR spectra were consistent with the presence of these types of phases and with a significant substitution of Al for Si in the tetrahedral chains of tobermorite. In fact, analyses of these C-A-S-H phases are consistent with the 0.2–0.3 Al/(Si+Al) ratio described in the literature. A major conclusion of this work is that the most typical C-S-H phase from the montmorillonite–cement interface reactivity is Al-tobermorite, at least in the absence of carbonation. The inhibition of C-A-S-H in the presence of carbonates is not complete as can be deduced from the long-term medium-cell experiments. Therefore, thermodynamic description of these phases should be performed, with a view to considering them in geochemical models that evaluate the performance of concrete and bentonite engineered barriers in a radioactive waste repository.

With respect to the common layered structure of C-A-S-H and montmorillonite, a structural interaction of the two phases may occur. This mechanism has been considered as an explanation of the hindrance of

FIG. 5. ^{29}Si MAS NMR spectra of: (A) medium cells; (B) small cells; and (C) batch experiments. Samples D1-C and D3 in small cells correspond to the sample located at the interface of mortar–bentonite and a sample in bentonite at 2 cm from the interface, respectively.

In the current work, the Q^1 signals, which indicate Si tetrahedra of the end chains, were not observed. A high Q^1/Q^2 ratio means that C-S-H structure is characterized by short chains of Si tetrahedra and is typical of jennite

TABLE 3. ²⁹Si MAS NMR chemical shifts (δ) from cement materials–bentonite interfaces in several experiments: HB4 and HB5 from medium-cell experiments; D-1C and D3 from the small-cell 5 mortar–bentonite interface; and a sample at 2 cm from the interface, respectively. Mont60 and 120: montmorillonite-portlandite batch experiments at 60 and 120°C at molar ratios of 2:1. Mmt indicates the untreated <2 μm size fraction of FEBEX bentonite.

Sample	δ Quartz (ppm)	δ Q³ (ppm)	δ Q²(0Al) (ppm)	δ Q²(1Al) (ppm)
Mmt		−93.8		
HB4		−93.3		
HB5		−93.6	Shoulder	
D1-C	−107.4	−93.5	−85.1	−81.4
D3		−93.6		
Mont60		−93.6	−85.3	
Mont120		−93.6	−86.4	−83.2

montmorillonite swelling at the cement materials–bentonite contacts.

REFERENCES

Andrade C., Martínez I., Castellote M. & Zuloaga P. (2006) Some principles of service life calculation of reinforcements and in situ corrosion monitoring by sensors in the radioactive waste containers of El Cabril disposal (Spain). *Journal of Nuclear Materials*, **358**, 82–95.

Blanc P., Bourbon X., Lassin A. & Gaucher E.C. (2010) Chemical model for cement-based materials: Temperature dependence of thermodynamic functions for nanocrystalline and crystalline C-S-H phases. *Cement and Concrete Research*, **40**, 851–866.

Brew D.R.M. & Glasser F.P. (2005) Synthesis and characterisation of magnesium silicate hydrate gels. *Cement and Concrete Research*, **35**, 85–98.

Brunet F., Bertani P., Charpentier T., Nonat A. & Virlet J. (2004) Application of 29Si homonuclear and 1H −29Si heteronuclear NMR correlation to structural studies of calcium silicate hydrates. *The Journal of Physical Chemistry B*, **108**, 15494–15502.

Caballero E., Jiménez de Cisneros C., Huertas F.J., Huertas F., Pozzuoli A. & Linares J. (2005) Bentonite from Cabo de Gata, Almería, Spain: A mineralogical and geochemical overview. *Clay Minerals*, **40**, 463–480.

Cong X. & Kirkpatrick R.J. (1996) 29Si MAS NMR study of the structure of calcium silicate hydrate. *Advanced Cement Based Materials*, **3**, 144–156.

Cuevas J., Vigil de la Villa R., Ramírez S., Sánchez L., Fernández R. & Leguey S. (2006) The alkaline reaction of FEBEX bentonite: A contribution to the study of the performance of bentonite/concrete engineered barrier systems. *Journal of Iberian Geology*, **32**, 151–174.

Cuevas J., Fernández R., Ruiz A.I., de Soto I.S., Vigil de la Villa R., Escribano A., Torres E., Villar M.V. & Turrero M.J. (2012) Mineral reaction front developed in a 4.5 years test for the study of concrete-bentonite interface. *Macla*, **16**, 128–129.

Cuevas J., Turrero M.J., Torres E., Fernández R., Ruiz A.I. & Escribano A. (2013) Laboratory tests at the interfaces: Results of small cells with mortar-bentonite-magnetite. 83 pp. PEBS Deliverable D2.3-3-2.

Cuevas J., Fernández R., Torres E., Escribano A., Ruiz A.I., Regadío M. & Turrero M.J. (2014a) An experimental approach to study the long-term alteration of compacted bentonite affected by cement degradation and iron corrosion products. *Proceedings of the International Conference on the Performance of Engineered Barriers: Backfill, Plugs and Seals*, German Geological Survey, BGR, pp. 161–166.

Cuevas J., Samper J., Turrero M.J. & Wieczorek K. (2014b) Impact of the geochemical evolution of bentonite barriers on repository safety functions – PEBS case 4. *Proceedings of the Proceedings International Conference on the Performance of Engineered Barriers: Backfill, Plugs and Seals*, German Geological Survey, BGR, pp. 35–42.

Cuevas J., Ruiz A.I., Fernández R., Torres E., Escribano A., Regadío M. & Turrero M.J. (2016) Lime mortar-compacted bentonite–magnetite interfaces: an experimental study focused to the understanding of the EBS long-term performance for high-level nuclear waste isolation DGR concept. *Applied Clay Science*, **124–125**, 79–93.

Dauzères A., Le Bescop, P., Cau-Dit-Coumes C., Brunet F., Bourbon X., Timonen J., Voutilainen M., Chomat L. & Sardini P. (2014) On the physico-chemical evolution of low-pH and CEM I cement pastes interacting with Callovo-Oxfordian pore water under its in situ CO_2 partial pressure. *Cement and Concrete Research*, **58**, 76–88.

Dauzères A., Le Bescop P., Sardini P. & Cau Dit Coumes C. (2010) Physico-chemical investigation of clayey/cement-based materials interaction in the context of geological waste disposal: Experimental approach and results. *Cement and Concrete Research*, **40**, 1327–1340.

de Jong B.H.W.S., van Hoek J., Veeman W.S. & Manson D.V. (1987) X-ray diffraction and ^{29}Si magic-angle-spinning NMR of opals: Incoherent long- and short-range order in opal-CT. *American Mineralogist*, **72**, 1195–1203.

Diamond S., White J.L. & Dolch W.L. (1963) Transformation of clay minerals by calcium hydroxide attack. *Proceedings of the 12th National Conference*, Atlanta, Georgia, USA, *Clays and Clay Minerals*, **12**, 359–379.

Fernández A.M., Baeyens B., Bradbury M. & Rivas P. (2004) Analysis of the porewater chemical composition of a Spanish compacted bentonite used in an engineered barrier. *Physics and Chemistry of the Earth*, **29**, 105–118.

Fernández R., Cuevas J., Sánchez L., Vigil de la Villa R. & Leguey S. (2006) Reactivity of the cement-bentonite interface with alkaline solutions using transport cells. *Applied Geochemistry*, **21**, 977–992.

Fernández R., González L., Ruiz A.I. & Cuevas J. (2014a) Nature of C-(A)-S-H phases formed in the reaction bentonite/portlandite. *Journal of Geochemistry*, **2014**, 1–8.

Fernández R., Rodríguez M., Vigil de la Villa R. & Cuevas J. (2010) Geochemical constraints on the stability of zeolites and C-S-H in the high pH reaction of bentonite. *Geochimica et Cosmochimica Acta*, **74**, 890–906.

Fernández R., Ruiz A.I. & Cuevas J. (2014b) The role of smectite composition on the hyperalkaline alteration of bentonite. *Applied Clay Science*, **95**, 83–94.

Gaucher E.C. & Blanc P. (2006) Cement/clay interactions – a review: Experiments, natural analogues, and modeling. *Waste Management*, **26**, 776–788.

Grandia F., Galíndez J.-M., Molinero J. & Arcos D. (2010) Evaluation of low-pH cement degradation in tunnel plugs and bottom plate systems in the frame of SR-Site. SKB Technical Report TR-10-62, 49 pp.

Henmi C. & Kusachi I. (1992) Clinotobermorite, $Ca_5Si_6(O,OH)_{18}\cdot5H_2O$, a new mineral from Fuka, Okayama prefecture, Japan. *Mineralogical Magazine*, **56**, 353–358.

Jackson M.D., Chae S.R., Mulcahy S.R., Meral C., Taylor R., Li P., Emwas A.-H., Moon J., Yoon S., Vola G., Wenk H.-R. & Monteiro P.J.M. (2013) Unlocking the secrets of Al-tobermorite in Roman seawater concrete. *American Mineralogist*, **98**, 1669–1687.

Jenni A., Mäder U., Lerouge C., Gaboreau S. & Schwyn B. (2014) In situ interaction between different concretes and Opalinus Clay. *Physics and Chemistry of the Earth, Parts A/B/C*, **70–71**, 71–83.

Komarneni S., Breval E., Miyake M. & Roy R. (1987) Cation-exchange properties of (Al+Na)-substituted synthetic tobermorites. *Clays and Clay Minerals*, **35**, 385–390.

Kulik D.A. (2011) Improving the structural consistency of C-S-H solid solution thermodynamic models. *Cement and Concrete Research*, **41**, 477–495.

Lippmaa E., Maegi M., Samoson A., Engelhardt G. & Grimmer A.R. (1980) Structural studies of silicates by solid-state high-resolution silicon-29 NMR. *Journal of the American Chemical Society,* **102**, 4889–4893.

Marty N.C.M., Tournassat C., Burnol A., Giffaut E. & Gaucher E.C. (2009) Influence of reaction kinetics and mesh refinement on the numerical modelling of concrete/clay interactions. *Journal of Hydrology*, **364**, 58–72.

Merlino S., Bonaccorsi E. & Armbruster T. (1999) Tobermorites: Their real structure and order-disorder (OD) character. *American Mineralogist*, **84**, 1613–1621.

Nonat A. (2004) The structure and stoichiometry of C-S-H. *Cement and Concrete Research*, **34**, 1521–1528.

Pardal X., Pochard I. & Nonat A. (2009) Experimental study of Si–Al substitution in calcium-silicate-hydrate (C-S-H) prepared under equilibrium conditions. *Cement and Concrete Research*, **39**, 637–643.

Pomakhina E., Deneele D., Gaillot A.-C., Paris M. & Ouvrard G. (2012) 29Si solid state NMR investigation of pozzolanic reaction occurring in lime-treated Ca-bentonite. *Cement and Concrete Research*, **42**, 626–632.

Rao S. & Rajasekaran G. (1996) Reaction products formed in lime-stabilized marine clays. *Journal of Geotechnical Engineering*, **122**, 329–336.

Richardson I.G., Brough A.R., Brydson R., Groves G.W. & Dobson C.M. (1993) Location of aluminum in substituted calcium silicate hydrate (C-S-H) gels as determined by 29Si and 27Al NMR and EELS. *Journal of the American Ceramic Society*, **76**, 2285–2288.

Roosz C., Grangeon S., Blanc P., Montouillout V., Lothenbach B., Henocq P., Giffaut E., Vieillard P. & Gaboreau S. (2015) Crystal structure of magnesium silicate hydrates (M-S-H): The relation with 2:1 Mg–Si phyllosilicates. *Cement and Concrete Research*, **73**, 228–237.

Russias J., Frizon F., Cau-Dit-Coumes C., Malchère A., Douillard T. & Joussot-Dubien C. (2008) Incorporation of aluminum into C-S-H structures: From synthesis to nanostructural characterization. *Journal of the American Ceramic Society*, **91**, 2337–2342.

Samper F.J., Montenegro L., Turrero M.J., Martín P.L., Garralón A., Cuevas J. & Fernández R. (2010) Technical Note 1: Design of new experiments. Pp. 10. PEBS Internal Deliverable D 3.4.2.

Sánchez L., Cuevas J., Ramírez S., Ruiz de León D., Fernández R., Vigil de la Villa R. & Leguey S. (2006) Reaction kinetics of FEBEX bentonite in hyperalkaline conditions resembling the cement-bentonite interface. *Applied Clay Science*, **33**, 125–141.

Savage D., Soler J.M., Yamaguchi K., Walker C., Honda A., Inagaki M., Watson C., Wilson J., Benbow S., Gaus I. & Rueedi J. (2011) A comparative study of the modelling of cement hydration and cement–rock laboratory experiments. *Applied Geochemistry*, **26**, 1138–1152.

Savage D., Walker C., Arthur R., Rochelle C., Oda C. & Takase H. (2007) Alteration of bentonite by hyperalkaline fluids: A review of the role of secondary minerals. *Physics and Chemistry of the Earth, Parts A/B/C*, **32**, 287–297.

Soler J.M. (2013) Reactive transport modeling of concrete-clay interaction during 15 years at the Tournemire Underground Rock Laboratory. *European Journal of Mineralogy*, **25**, 639–654.

Soler J.M. & Mäder U.K. (2010) Cement-rock interaction: Infiltration of a high-pH solution into a fractured granite core. *Geologica Acta*, **8**, 221–233.

Sun G.K., Young J.F. & Kirkpatrick R.J. (2006) The role of Al in C-S-H: NMR, XRD, and compositional results for precipitated samples. *Cement and Concrete Research*, **36**, 18–29.

Thompson J.G. (1984) ^{29}Si and ^{27}Al nuclear magnetic resonance spectroscopy of 2:1 clay minerals. *Clay Minerals*, **19**, 229–236.

Torres E., Escribano A., Turrero M.J., Martín P.L., Peña J. & Villar M.V. (2009) Temporal evolution of the concrete-bentonite system under repository conditions. *Proceedings of the Materials Research Society Symposium Proceedings,* Boston, Massachusetts, USA, pp. 295–300.

Torres E., Turrero M.J., Escribano A., Fernández R., Ruiz A.I. & Cuevas J. (2014) Temporal evolution of the Fe/FEBEX bentonite system under simultaneous hydration and heating – results up to seven years. *Proceedings of the International Conference on the Performance of Engineered Barriers: Backfill, Plugs and Seals, 2014*, German Geological Survey, BGR, pp. 153–160.

Turrero M.J., Villar M.V., Torres E., EscribanoA., Cuevas J., Fernández R., Ruiz A.I., Vigil de la Villa R. & de Soto I.S. (2011) Laboratory tests at the interfaces: First results on the dismantling of tests FB3 and HB4. Pp. 64. PEBS Deliverable D2.3-3-1.

U.S. Deparment of Energy (2014) Evaluation of options for permanent geologic disposal of spent nuclear fuel and high-level radioactive waste. Pp. 89. Used Fuel Disposition Campaign, Revision 1. SAND2014-0187P, Sandia National Laboratories. FCRD-UFD-2013-000371.

Ufer K., Roth G., Kleeberg R., Stanjek H., Dohrmann R. & Bergmann J. (2004) Description of X-ray powder pattern of turbostratically disordered layer structures with a Rietveld compatible approach. *Zeitschrift fur Kristallographie*, **219**, 519–527.

Villar M.V., Pérez del Villar L., Martín P.L., Pelayo M., Fernández A.M., Garralón A., Cuevas J., Leguey S., Caballero E., Huertas F.J., Jiménez de Cisneros C., Linares J., Reyes E., Delgado A., Fernández-Soler J. M. & Astudillo J. (2006) The study of Spanish clays for their use as sealing materials in nuclear waste repositories: 20 years of progress. *Journal of Iberian Geology*, **32**, 15–36.